

18 Abstract

19 In the Anthropocene, humans are the largest drivers of change in vegetation fire regimes.
20 Humans influence fire regimes both directly, by starting, managing and extinguishing fires, and
21 also indirectly by altering fuel composition and connectivity. However, whilst vegetation fire is a
22 coupled socio-ecological process, representation of human influences on fire regimes in global-
23 scale modelling remains limited. This places a fundamental constraint on our ability to
24 understand how human and natural processes combine to create observed patterns of vegetation
25 fire, and how such processes may interact under future scenarios of socioeconomic and
26 environmental change. Here, we respond to this challenge by presenting a novel integration of
27 two global and process-based models. The first is the Wildfire Human Agency Model
28 (WHAM!), which draws on agent-based approaches to represent anthropogenic fire use and
29 management. The second is JULES-INFERNO, a fire-enabled dynamic global vegetation model,
30 which takes a physically-grounded approach to the representation of vegetation-fire dynamics.
31 The WHAM-INFERNO combined model suggests that as much as half of all global burned area
32 is generated by managed anthropogenic fires – typically small fires that are lit and then spread
33 according to land user objectives. Furthermore, we demonstrate that including representation of
34 managed anthropogenic fires in a coupled socio-ecological simulation can improve
35 understanding of the drivers of unmanaged wildfires. Overall, findings presented here have
36 substantial implications for understanding of present-day and future fire regimes, indicating that
37 socio-economic change may be as important as climate change in determining the future
38 trajectory of fire on Earth.

39

40 Plain Language Summary

41 For millennia, humans have used fire as a tool to manage land and they continue to do so across
42 the world today. However, global-scale models which are used to understand how vegetation fire
43 may respond to climate change have not yet robustly accounted for this. So, we built a new
44 model that represents how humans use and manage fire globally and coupled it with a global fire
45 model. We find that improved representation of human impacts on fire significantly improves the
46 model and sheds new light on what is driving change in vegetation fire globally. In particular,
47 our results suggest current global fire models may have underestimated the sensitivity of fire to
48 climate change.

49

50 **1 Introduction**

51 Vegetation fire is a coupled socio-ecological process, in which humans are the largest
52 driver of change in its global distribution (Andela et al., 2017; Kelley et al., 2019). Perhaps the
53 central example of this is that, whilst the planet has warmed under recent anthropogenic climate
54 change, the area burned globally each year has decreased, particularly in savannas and grasslands
55 (Chen et al., 2023). Drivers of this phenomenon are complex and uncertain (Zubkova et al.,
56 2023), ranging from cropland conversion (Andela et al., 2017) to changes in anthropogenic fire
57 use (Smith et al., 2022), from increased grazing intensity (Archibald & Hempson, 2016) to the
58 CO₂ fertilisation effect (Ripley et al., 2022; Stevens et al., 2016). A lack of clarity around the
59 drivers of declining global burned area has made attribution of changes in global fire regimes a
60 significant challenge (Jones et al., 2022). This, in turn, limits understanding of how fire may
61 evolve in the future, including its potential role as a positive feedback to climate change (Lasslop
62 et al., 2019).

63 At the heart of this uncertainty are the huge diversity of ways in which humans use and
64 manage fire. Human fire use ranges from burning of agricultural residues in intensive land use
65 systems (Kumar et al., 2023) to cultural uses such as religious ceremonies (Smith et al., 2022).
66 Human fire management is similarly diverse, ranging from pro-active indigenous ‘patch-
67 burning’ methods (Laris, 2002) to industrial fire suppression. As such, fire can broadly be
68 categorised into managed or ‘landscape’ fires - which are typically small, controlled, and can be
69 beneficial to humans - and unmanaged wildfires, which are larger and burn more intensely
70 (UNEP 2022). Furthermore, human fire use is itself undergoing substantial change, with shifts
71 away from more subsistence-oriented fire uses (Smith et al., 2022) and possibly an overall
72 decline in fire use driven by agricultural intensification (Perkins et al., 2023). Consequently,
73 Shuman et al., (2022) argue that incorporating managed fire into models at all spatial scales is an
74 important step towards equipping fire science for the Anthropocene.

75 In addition to direct anthropogenic influences on fire, humans also have many indirect
76 influences on fire regimes. For example, multiple authors have argued that anthropogenic
77 fragmentation of vegetated landscapes is a key process shaping the evolution of global fire
78 (Archibald et al., 2012; Driscoll et al., 2021; Harrison et al., 2021). Fragmentation can have
79 opposite effects across ecosystems – with logging and degradation increasing fire in otherwise
80 fire-independent forests, and reduced fuel connectivity decreasing burned area in grassland and
81 savannah ecosystems (Rosan et al., 2022). As such, understanding the drivers of change within
82 global fire regimes requires consideration not only of biophysical factors, but also of both direct
83 and indirect human impacts.

84 Global-scale fire models have struggled to reproduce the observed decline in global
85 burned area (Hantson et al., 2020). Indeed, in the first intercomparison project of the global fire
86 model community (FireMIP; Rabin et al., 2017), models largely disagreed about both centennial
87 trends, and more recent decadal trends, in global burned area (Teckentrup et al., 2019).
88 Underlying this lack of consensus have been substantial limitations in the representation of
89 human impacts on the fire modules of dynamic global vegetation models (DGVMs; Ford et al.,
90 2021). Typically, these have been restricted to global functions relating population density to
91 numbers of fires in satellite observations (Rabin et al., 2017). This ignores the diversity of human
92 fire use and management, and hence limits the capability of DGVMs to advance understanding
93 of socio-ecological dynamics of present-day fire regimes and how human and biophysical factors
94 may interact in the future (Shuman et al., 2022).

95 The Wildfire Human Agency Model (WHAM!; Perkins et al., 2023) is the first formal
96 model to represent present-day anthropogenic fire use and management at global scale. Drawing
97 on agent-based approaches, WHAM! is a geospatial behavioural model that captures the
98 underlying land system drivers of anthropogenic fire use and management to simulate human fire
99 use decision-making from the bottom-up (Perkins et al., 2022). As WHAM! only represents
100 human influences on global fire regimes, it was designed to be integrated with fire-enabled
101 DGVMs, such as the JULES-INFERNO model (Mangeon et al., 2016), which capture the
102 biophysical drivers of fire. Here we present the first coupling between WHAM! and JULES-
103 INFERNO, such that biophysical, direct and indirect human drivers of fire regimes are all
104 explicitly represented in an integrated simulation for the first time.

105 WHAM! takes its empirical basis from the Database of Anthropogenic Fire Impacts
106 (DAFI; Perkins & Millington, 2021). DAFI is the product of a literature meta-analysis of 1809
107 case studies from 504 academic papers, government and NGO reports (Millington et al., 2022).
108 This dataset addresses a previous barrier to improved representation of anthropogenic fire in
109 DGVMs: the lack of a systematic data set on which to base new parameterisations (Forkel et al.,
110 2019). Alongside development of DAFI, the 5th version of the Global Fire Emissions Database
111 (GFED5; Chen et al., 2023) accounts for smaller fires than previous versions and therefore
112 enables more robust evaluation of global-scale modelling of human fire interactions. Previous
113 iterations of GFED have been based on a combination of MODIS for burned area and VIRS for
114 active fire detection (Giglio et al., 2013). As such, they have not been able to systematically
115 detect anthropogenic fires: DAFI suggests that >50% of anthropogenic fires are smaller than the
116 21ha threshold above which MODIS can detect (Millington et al., 2022). GFED5 incorporates
117 higher resolution remote sensing (principally from Landsat and Sentinel-2), and hence is much
118 more effective at capturing small fires: global burned area in GFED5 is a 61% increase over
119 GFED4s (Chen et al., 2023). Therefore, with DAFI providing an empirical-basis for bottom-up
120 modelling of human-fire interactions, and GFED5 better able to detect them from space, a
121 comprehensive and empirically-grounded assessment of the role of managed anthropogenic fire
122 in global fire regimes is now possible.

123 This paper presents the integration of WHAM! with JULES-INFERNO and its
124 application to understand the spatiotemporal drivers of global fire regimes. Section 2 (Methods)
125 focuses on describing the integration of outputs from the two models. Model calibration is
126 described briefly in the main text with further details provided in Supplementary Information A.
127 In Section 3 (Results), we present a brief evaluation of the outputs of the coupled model to
128 establish its credibility, before focusing on understanding how human and biophysical factors
129 combine to produce observed distributions of fire globally. Discussion (section 4) focuses on
130 insights relevant to the question of declining global burned area, and in particular to
131 understanding the relative contribution of direct human influences (starting and suppressing
132 fires), indirect human influences (i.e. landscape fragmentation) and biophysical factors (i.e.
133 climate and vegetation flammability).

134

135 2 Methods

136 Our methods are presented in five sections, which respectively describe the inputs,
137 structure, calibration, evaluation, and analysis of the WHAM-JULES-INFERNO combined
138 model (hereafter WHAM-INFERNO). A schematic overview of the processes represented in
139 WHAM-INFERNO is presented in Figure 1. Calculations of the fire regime at each timestep
140 combine three elements: 1) WHAM! outputs for managed and unmanaged anthropogenic fires
141 and fire suppression; 2) JULES-INFERNO outputs for lightning ignitions, flammability and
142 plant functional types; and 3) a representation of vegetation fragmentation derived from
143 secondary data and WHAM! outputs for logging. These are each detailed further in Section 2.1.

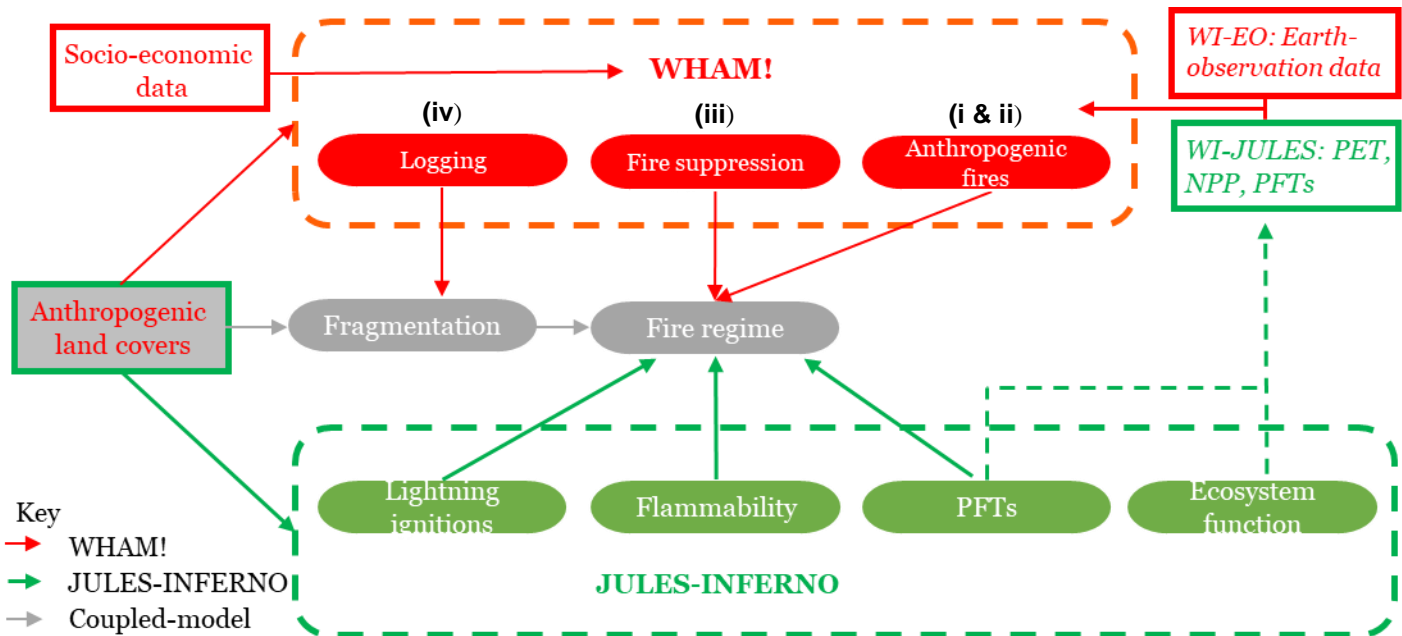
144 Importantly, two versions of WHAM-INFERNO are presented and assessed: WHAM-
145 INFERNO-JULES (hereafter WI-JULES) and WHAM-INFERNO-Earth Observation (hereafter
146 WI-EO). The difference between these two versions is that in WI-JULES, WHAM! is
147 parameterised using biophysical inputs directly from JULES, whilst in WI-EO, WHAM! takes
148 these inputs from remote sensing. Specifically, inputs for potential evapotranspiration, net
149 primary production and the bare soil fraction are replaced with Earth observation data. The
150 differences between these two versions of WHAM! are described in detail in Perkins et al. (2023;
151 Supplementary Information A).

152 The primary purpose of the comparison of WI-JULES and WI-EO is to allow
153 interrogation of the robustness of inferences made about the drivers of global fire regimes. For
154 example, if trends are identified in WI-JULES but not in WI-EO, then they may be attributable to
155 underlying model error in JULES' representation of ecosystem dynamics. Similarly, assessing
156 the difference in performance (as measured against GFED5) allows exploration of how far
157 underlying error in the hydrological and vegetation outputs of DGVMs may constrain the
158 capacity of their fire modules to reproduce remotely sensed observations (Hantson et al., 2020).

159 Code to run and analyse WHAM-INFERNO is written in R version 4.2.2 (R Core Team
160 2022), using the 'raster' library version 3.6-20 (Hijmans et al., 2023). Code and data to run and
161 analyse outputs of both versions of WHAM-INFERNO are made available on Zenodo (Perkins
162 et al., 2023b).

163 2.1 Inputs to the coupled model

164 WHAM-INFERNO takes inputs from WHAM!, JULES-INFERNO and from secondary
165 data sources. Each of these inputs are described in turn below (Sections 2.1.1-2.1.3), and an
166 overview is given in Table 1. WHAM! outputs are annual, whilst as per results in the sixth
167 coupled model intercomparison project (CMIP6), JULES-INFERNO outputs are aggregated
168 monthly means. Therefore, WHAM-INFERNO runs at a monthly timestep, with WHAM!
169 outputs for a given year assumed to be uniformly distributed across calendar months.



170 **Figure 1:** Processes represented in the WHAM-INFERNO combined model. Solid arrows denote
 171 dynamic model calculations, whilst dashed lines denote static exchange of information. Socio-
 172 economic data and biophysical inputs to WHAM! (Potential Evapotranspiration (PET), Net
 173 Primary Production (NPP) and Plant Functional Types (PFTs)) are passed offline. In WHAM-
 174 INFERNO-JULES (WI-JULES) these data are taken from JULES outputs, whilst in WHAM-
 175 INFERNO-Earth Observation (WI-EO) PET and NPP inputs are taken from remote sensing.
 176 Roman numerals (i-iv) correspond to numbers given in section 2.1.1 of the text.

177 2.1.1 WHAM! inputs to the coupled model

178 WHAM! inputs to the coupled model comprise i) managed burned area as a fraction of
 179 each cell, ii) numbers of unmanaged fires (count $\text{km}^{-2} \text{yr}^{-1}$), iii) fire suppression intensity (0-1),
 180 and iv) the presence of selective logging as a fraction of the tree cover in each cell (see
 181 corresponding numerals in Figure 1). WHAM! inputs used were those presented in Perkins et al.,
 182 (2023).

183 2.1.2 JULES-INFERNO inputs to the coupled model

184 INFERNO (Mangeon et al., 2016) is the fire module of the JULES dynamic global
 185 vegetation model. INFERNO calculates burned area from fires with two key components. The
 186 first is mean global burned area per fire per Plant Functional Type (PFT), a set of PFT-specific
 187 model free parameters. Model parameters for burned area per PFT were as in Burton et al.
 188 (2019). The second component of INFERNO burned area calculations is fuel flammability,
 189 which INFERNO calculates as a function of leaf carbon and soil carbon pools, temperature,
 190 relative humidity, precipitation, and soil moisture (Mangeon et al., 2016). Flammability is
 191 therefore important in capturing the impact of both climate and spatial heterogeneity in
 192 vegetation on fire regimes. Flammability is calculated per PFT in each model pixel at each
 193 timestep. JULES outputs are from the model set-up used in CMIP6 (Wiltshire et al., 2020).

194 2.1.3 Ancillary inputs to the coupled model from secondary data

195 In addition to the calculations from the two models, three sets of secondary data were
 196 used as inputs: lightning ground strikes, anthropogenic land covers – cropland, pasture,
 197 rangeland and urban – and road density. Firstly, as in JULES-INFERNNO standalone (Mathison et
 198 al., 2023), counts of lightning strikes were sourced from the Lightning Imaging Sensor—Optical
 199 Transient Detector (LIS/OTD, Christian et al., 2003). Secondly, as in CMIP6, anthropogenic
 200 land cover was taken from the LUH2 dataset (Hurtt et al., 2020). Finally, Haas et al. (2022)
 201 demonstrated that road density was effective in capturing vegetation fragmentation effects on fire
 202 regimes at global scale; road density data were therefore taken from the GRIP global road
 203 database (Meijer et al., 2018).

204

205 **Table 1:** Overview of inputs to the WHAM!-INFERNNO combined model. PFT is plant
 206 functional type. Data inputs for lightning strikes, road density and anthropogenic land covers
 207 were rescaled to the resolution of WHAM!-INFERNNO (1.875° x 1.25°). Differing temporal
 208 resolutions of inputs were reconciled as noted in Section 2.1.

209

Coupled model input	Source	Units	Temporal resolution
Managed burned area	WHAM!	Cell fraction (0-1)	Annual
Unmanaged anthropogenic fires	WHAM!	Fires km ⁻²	Annual
Fire suppression	WHAM!	Cell fraction (0-1)	Annual
Selective logging	WHAM!	Cell fraction (0-1)	Annual
Distribution of PFTs	JULES-INFERNNO	Cell fraction (0-1)	Monthly
Flammability per PFT	JULES-INFERNNO	Dimensionless (0-1)	Monthly
Burned area per fire per PFT	JULES-INFERNNO	km ²	Fixed (n/a)
Lightning – ground strikes	Christian et al., (2003)	strikes km ⁻²	Fixed (single daily mean)
Road density	Meijer et al., (2018)	m ² km ⁻²	Annual
Anthropogenic land cover	Hurtt et al., (2020)	Cell fraction (0-1)	Annual

210

211

212 2.2 WHAM-INFERNO Structure

213 The coupled WHAM-INFERNO model is a ‘prescribed’ model coupling (sensu Robinson
 214 et al., 2018) such that whilst simulations of global burned area depend on calculations involving
 215 outputs of both models, dynamic information transfer is only one way - from WHAM! to
 216 INFERNO (see Section 2.2.1). Specifically, for each simulated year, annual burned area from
 217 managed fire is taken directly from WHAM!, with $\frac{1}{12}$ assigned to each calendar month. But to
 218 calculate unmanaged fire burned area, the original JULES-INFERNO calculations are modified
 219 by the number of anthropogenic fires ($\text{km}^{-2} \text{yr}^{-1}$) provided by WHAM!. Therefore, description of
 220 model coupling here first describes calculation of burned area from unmanaged fires (Section
 221 2.2.1). Then, as burned area from unmanaged fires is also impacted by anthropogenic landscape
 222 fragmentation, the representation of such processes is then described in Section 2.2.2. Finally,
 223 the calculation of overall burned area combining both managed and unmanaged fire is described
 224 in Section 2.2.3.

225 2.2.1 Unmanaged fire

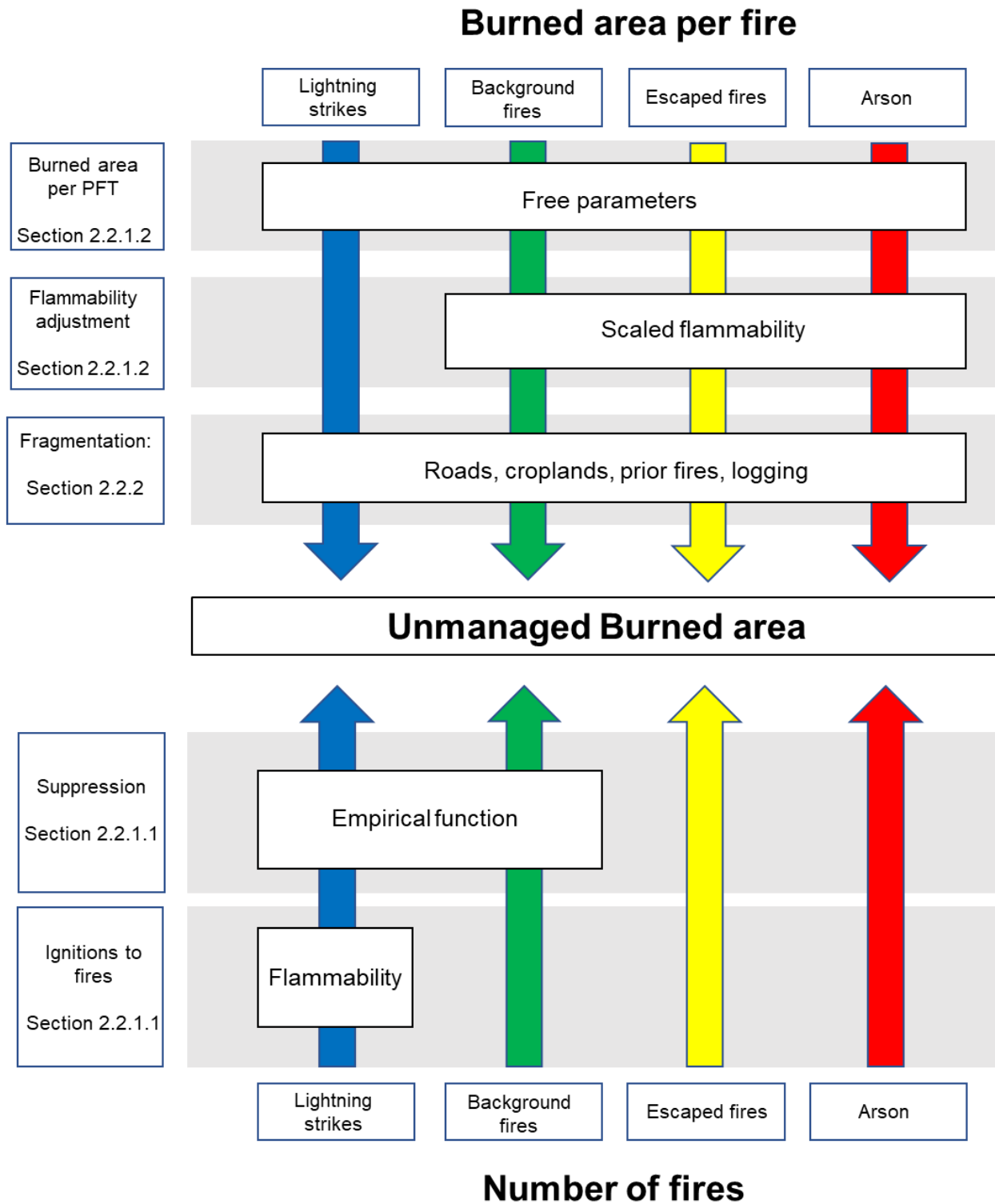
226 The calculation of burned area from unmanaged fires is presented in two parts: firstly the
 227 calculation of numbers of unmanaged fires, and secondly the calculation of their respective
 228 burned area. An overview of this process is given in Figure 2.

229 2.2.1.1 Number of fires

230 In the original Mangeon et al. (2016) conception of INFERNO, the numbers of ignitions
 231 from lightning strikes are calculated as follows:

$$232 \quad I_L = 7.7 \times \textit{Lightning} \times (1 - \textit{Suppression}) \quad (1)$$

234 where I_L is the number of ignitions from lightning strikes in a given model timestep, *Lightning*
 235 is the number of lightning strikes and *Suppression* is a population density-dependent
 236 suppression function. The structure of this calculation is retained with two changes: firstly, the
 237 suppression function is replaced with an empirically-defined representation of suppression
 238 intensity (Section 2.2.2); and secondly the empirically-defined linear scaling parameter (=7.7)
 239 from Mangeon et al. (2016) is replaced with a free parameter (λ) to allow re-calibration. A
 240 complete set of model free parameters is given in Supplementary Information Table S1.



241 **Figure 2:** Calculation of burned area from unmanaged fires in the WHAM-INFERNO combined
 242 model.
 243

244 In the WHAM-INFERNO combined model, calculation of lightning fires is integrated
245 with unmanaged anthropogenic fire numbers from WHAM! as follows:

$$246 \quad \text{Fires}_{UM} = Arson + Escaped + (1 - Suppression) * (Background + Lightning) \quad (2)$$

248 where $Fires_{UM}$ is the annual number of unmanaged fires per grid box per year, *Arson* and
249 *Escaped* fire numbers are the number of fires $\text{km}^{-2} \text{yr}^{-1}$ taken from WHAM! outputs, and
250 *Lightning* is the number of lightning fires calculated from mean daily ground strikes as in
251 equation (1). Finally, *Background*, is a small globally constant rate used to capture fires that
252 are not arson, lightning or escaped managed fires. The constant rate maintains an aspect of
253 INFERNO, in which a uniform ‘ignition’ rate is an option.

254 Fire suppression in the coupled model (Section 2.2.2) is applied to background and
255 lightning fires, but not to arson and escaped fires. This is for ontological reasons, as follows.
256 INFERNO assumes that suppressed *ignitions* have no burned area. However, in DAFI, the
257 database used to develop WHAM!’s calculation of arson and escaped *fires*, numbers of *fires* are
258 recorded, therefore by definition these have burned area > 0 . As such, it is illogical to apply
259 modelled suppression to them. By contrast, as the background rate was calculated using a
260 constant, clearly this did not account for the impact of suppression. Similarly, lightning remains
261 calculated based on *ignitions* rather than *fires* and hence could be suppressed before beginning to
262 burn.

263 2.2.1.2 Burned area per unmanaged fire

264 After calculation of the numbers of unmanaged fires per pixel ($Fires_{UM}$), these are then
265 converted to burned area. In its original conception, INFERNO calculates the number of fires as:

$$266 \quad \text{Fires} = Ignitions * Flammability \quad (3)$$

269 In other words, both humans and lightning are conceptualised as producing ignitions,
270 which may or may not become fires based on the flammability of the surrounding vegetation. By
271 contrast, because most human fires are started deliberately, WHAM! does not output numbers of
272 *ignitions*, but numbers of *fires* directly (Figure 2). However, whilst vegetation flammability plays
273 the ontological role of translating ignitions to fires in INFERNO, it also plays an important
274 functional role: capturing geographic variation in the capacity and tendency of the vegetation to
275 sustain unmanaged fire. This is because INFERNO calculates burned area per fire with a simple
276 global mean value per Plant Functional Type. Therefore, simply removing flammability from the
277 calculation and taking numbers of unmanaged fires from WHAM! was not possible.

278

279 The solution adopted is to multiply WHAM! unmanaged fires by INFERNO
 280 flammability, but to rescale with a free parameter. This leaves a burned area calculation from
 281 unmanaged fires of:

282

$$283 \quad BA_{UM} = Fires_{UM} * \Phi * \sum_{PFT=1}^{PFT=n} PFT * Flammability_{PFT} * BA_{PFT} \quad (4)$$

284 where BA_{UM} is the annual burned area from unmanaged fires as a fraction of each model pixel;
 285 PFT is the fraction of each model pixel (0-1) occupied by a given PFT; $Flammability_{PFT}$ is a
 286 PFT-specific dimensionless adjustment (0-1) reflecting spatiotemporal differences in the
 287 combustibility of vegetation; BA_{PFT} is the PFT-specific mean burned area per fire from JULES-
 288 INFERNO; and Φ is a scaling factor reflecting the differing model ontologies of WHAM! and
 289 JULES-INFERNO.

290 2.2.2 Fragmentation

291 The impact of landscape fragmentation effects was restricted to unmanaged fires;
 292 managed burned area was not altered for fragmentation effects, as these would already be
 293 implicitly accounted for in the observations captured in DAFI. Representation of fragmentation
 294 is done in three ways. Firstly, as WHAM! accounts for anthropogenic cropland fires, to account
 295 for the role of cropland conversion in fragmenting more flammable fuels, burned area per
 296 unmanaged fire was set to 0 for cropland PFTs.

297 Secondly, Haas et al., (2022) demonstrate the importance of road density in reducing both
 298 fire sizes and burned area. This finding was implemented in the coupled model by adjusting
 299 burned area per fire with a simple negative exponential function:

300

$$301 \quad BA_{UM_frag} = BA_{UM} * \left(1 - \frac{\ln(RD)}{\rho} \right) \quad (5)$$

302 where BA_{UM} and BA_{UM_frag} are annual burned area per pixel (0-1) from unmanaged fire before
 303 and after adjustment for fragmentation effects, RD is road density and ρ a free parameter.

304 By contrast, logging of wet, fire-prone forests can lead to increased fire (both numbers of
 305 fires and fire size), as gaps in the canopy lead to drying on the forest floor (Cochrane & Barber,
 306 2009; Lapola et al., 2023). A simple representation of this was implemented by increasing the
 307 mean burned area per fire for broadleaf tree PFTs given the presence of the Logging AFT in
 308 WHAM! outputs. The values of mean burned area for broadleaf tree PFTs therefore become:

309

$$310 \quad BA_{broadleaf|logging} = BA_{broadleaf} * \Lambda(Logging) \quad (6)$$

311 where $BA_{broadleaf}$ is the burned area per fire for broadleaf tree PFTs; $BA_{broadleaf|logging}$ is
 312 this parameter value when adjusted for logging, $Logging$ is the fraction of tree cover in a cell
 313 occupied by WHAM's logging AFT, and Λ a free parameter.

314 2.2.3 Combining managed and unmanaged fire

315 JULES-INFERNO typically runs at a timestep of between 30-60 minutes (Clark et al.,
 316 2011). This is required for the stability of model equations and has the advantage of capturing
 317 temporal fluctuations in vegetation flammability. As such, INFERNO increases the amount of
 318 bare soil in a given model pixel when a fire burns, which reduces fuel availability and the
 319 amount of area burned from subsequent fires until vegetation resprouts (Burton et al., 2019).
 320 However, as it is not meaningful to model human land use decision-making at such short
 321 durations (Arneth et al., 2014), managed fire is output at an annual timestep by WHAM!. For
 322 these reasons, calculating the combined burned area of managed and unmanaged fires requires an
 323 adjustment to account for the effect of preceding fires:

$$324 \quad 325 \quad BA_{tot} = BA_{Managed} + BA_{UM} * \gamma \quad (7)$$

326 where $BA_{Managed}$ is burned area from managed fire, BA_{tot} is total burned area and γ a function
 327 representing the impact of preceding fires on unmanaged burned area. Managed fire was not
 328 adjusted for effects of antecedent fire for several reasons: firstly, because WHAM! has its own
 329 internal calculation for including fuel limitations in agent calculations; secondly, because
 330 WHAM! outputs are empirically grounded, derived from data that would capture such
 331 limitations to a degree. Thirdly, many managed anthropogenic fires are lit to reduce the intensity
 332 and spread of unmanaged fire (e.g. prescribed fire or indigenous patch burning mosaics). The γ
 333 function was calculated using a linear function after a threshold:

$$334 \quad 335 \quad \gamma = \begin{cases} 1 & \text{if } BA_{UM} \leq \alpha \\ \beta & \text{otherwise} \end{cases} \quad (8)$$

336 where α is a free parameter representing a threshold burned fraction of a cell below which fuel
 337 availability is not limiting, whilst β is a further free parameter capturing the rate of decay in
 338 burned area once this threshold is reached. This functional form was chosen as it approximates
 339 the behaviour observed by Archibald et al. (2012), who explored the impact of fragmentation on
 340 burned area in flammable ecosystems.

341

342 2.3 WHAM-INFERNO Calibration

343 The model structure set out in Section 2.2 resulted in 20 free parameters (Supplementary
 344 Table S1), which formed the basis of a perturbed parameter ensemble for model calibration. A
 345 total of 10,000 perturbed parameter sets were created with a maximin latin hypercube sampling
 346 design (Carnell 2022). Using the resulting parameter sets, 10,000 model runs were conducted
 347 (i.e. one for each perturbed parameter combination) for both versions of the WHAM-INFERNO
 348 ensemble.

349

350 The outputs of each run were compared with the recent GFED5 global burned area
351 product (Chen et al., 2023). Firstly, ‘implausible’ parameter sets were ruled using history
352 matching with the overall magnitude of global burned area in GFED5. Remaining parameter sets
353 were then treated as ‘not ruled out yet’ (NROY; Rougier & Beven, 2013). Secondly, as well as
354 global burned area, Pearson’s correlation (r) was calculated with a square root transformation
355 applied. These two metrics were those used in the FireMIP (Teckentrup et al., 2019), and hence
356 were adopted here to define a pareto-optimal parameter space capturing the trade-offs in
357 maximising performance against each metric. This approach allows, firstly, the evaluation of
358 different model processes in capturing observed fire regimes of the recent past, and secondly
359 overall evaluation of the performance of the WHAM-INFERNO ensemble. The mean outputs of
360 WI-JULES and WI-EO in the pareto parameter space then formed the basis of further analysis.
361 Fuller detail of model calibration is given in Supplementary Information A.

363 2.4 WHAM-INFERNO Evaluation

364 WHAM-INFERNO is evaluated in two broad ways, firstly by output corroboration
365 through comparison of model outputs with remotely sensed burned area from GFED5 (as
366 described above) and secondly by model benchmarking against a null or baseline model. The
367 baseline model was an offline version of INFERNO (as presented in Mangeon et al., 2016). As
368 INFERNO was originally calibrated using GFED4 data, in which burned area was 49% lower
369 than the more recent GFED5 burned area product, a process of recalibration required. The re-
370 calibration of this INFERNO offline model (hereafter, ‘baseline model’) followed broadly the
371 same steps as WHAM-INFERNO combined model: 10,000 parameter sets were used to define a
372 perturbed parameter ensemble, from which both NROY and pareto-optimal parameter spaces
373 were defined using GFED5 burned area. Detailed description of the setup of the baseline model,
374 including how its free parameters differ from WHAM-INFERNO, is described in Supplementary
375 Information A.

377 2.5 Historical run setup and analysis

378 As with the WHAM! standalone historical simulations presented in Perkins et al. (2023),
379 WHAM-INFERNO runs span 1990-2014. These two years mark the beginning of the data
380 recorded in the DAFI database of global anthropogenic fire impacts (i.e. 1990; Millington et al.,
381 2022) that was used to parameterise WHAM!, and the end of the CMIP6 historical period (i.e.
382 2014), respectively. Both models were run at the spatial resolution that JULES-INFERNO
383 adopted in the FireMIP ($1.875^\circ \times 1.25^\circ$). Model outputs are evaluated during the overlapping
384 period in WHAM-INFERNO historical runs and the GFED5 record (2001-2014); GFED5 data
385 were aggregated to the spatial resolution of WHAM-INFERNO.

386 Analysis of outputs focuses on understanding spatial and temporal variation in the drivers
387 of global fire regimes. Spatial analysis focuses on understanding how managed anthropogenic
388 fire and unmanaged fire combine to produce observed fire regimes across global regions.
389 Similarly, temporal analysis first assessed how far managed fire and unmanaged fire contribute
390 to interannual variability in fire regimes. This was calculated by detrending the global total
391 burned area from GFED5 and WHAM-INFERNO model outputs before calculating the
392 correlation and standard deviation of the residual variabilities.

393 Then, drivers of longer-term (decadal) change were assessed. Perkins et al. (2023)
394 present analysis of the drivers of change in WHAM! managed fire outputs. Results pointed to
395 land use intensification as a global dampening effect on fire use, whilst conversely land use
396 extensification - particularly for livestock farming - led to increased fire use. Therefore, analysis
397 of temporal trends here focuses on change in unmanaged fire in relation to the human and
398 physical drivers represented in the coupled models. These are annual changes in numbers of
399 unmanaged fires, road density (fragmentation; Haas et al., 2022), vegetation flammability, fire
400 suppression and cropland conversion. The relative influence of these drivers was assessed at a
401 pixel-level firstly by comparing the Kendall's Tau correlations of their interannual changes with
402 interannual change in unmanaged burned area (for each of WI-JULES and WI-EO). Secondly,
403 using these same independent variables, linear models of pixel-level change in unmanaged
404 burned area were fit for both interannual and overall change between 2001-2014. T-values of the
405 independent variables were used to assess the relative strength of their relationships to changes in
406 unmanaged burned area.

407

408 **3 Results**

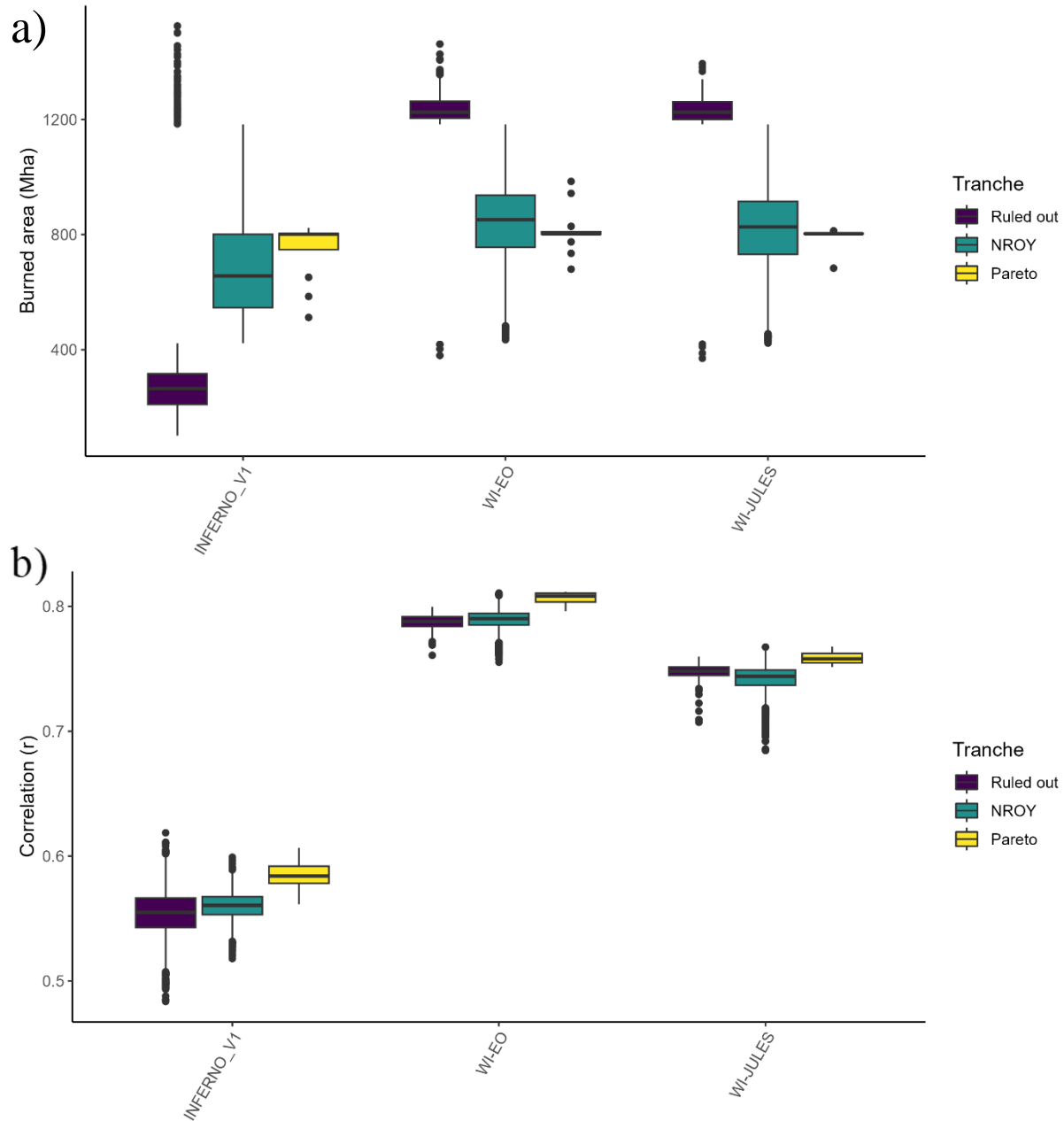
409 **3.1 Model evaluation**

410 Measured by correlation with the GFED5 record during 2001-2014, both WI-JULES and
411 WI-EO perform significantly better than the baseline model (Z Tests; both $p < 0.001$, $n = 10, 14$).
412 Specifically, the mean correlation of the pareto-optimal parameter space is 0.81 for WI-EO and
413 0.76 for WI-JULES, compared with 0.58 for the baseline model (Figure 3). This result also
414 compares favourably with INFERNO v1.0 presented in the FireMIP, in which INFERNO had a
415 correlation of 0.70 against GFEDv4 and 0.64 against GFEDv4s (Teckentrup et al., 2019). As
416 such, inclusion of WHAM! seemingly improves INFERNO both in an absolute sense, when
417 compared to GFED5, but also relatively against INFERNO's performance based on the
418 observational data available at the time of its original development.

419 Furthermore, almost 70% of the baseline model ensemble's runs are ruled out, primarily
420 due to simulating burned area too low to achieve acceptable coherence with the GFED5 record
421 (mean of ruled out runs was 276 Mha vs 802 Mha in GFED5). By contrast, only 182 of WI-EO
422 and 124 of WI-JULES runs are ruled out. In the pareto parameter space, WI-EO has a slight
423 overprediction bias (+11 Mha) and WI-JULES has a slight underprediction bias (-10 Mha),
424 compared to a bias of -52 Mha in the baseline model. Overall, we conclude that the WHAM
425 integration improves the structural capacity of INFERNO to capture the magnitude and
426 distribution of global fire regimes.

427

428



429 **Figure 3:** Outputs of WHAM-INFERNO in comparison with a baseline model (INFERNNO_V1):
 430 a) simulated global burned area and b) Pearson correlation with GFED5. For burned area, the
 431 baseline model has many runs ruled out for burned area being too low in comparison with
 432 GFED5, whilst in both versions of WHAM-INFERNO a smaller number of runs are ruled out.
 433 The two versions of WHAM-INFERNO both produce higher correlations than the baseline
 434 model across all three tranches of parameter sets (ruled out, NROY and pareto-optimal). NROY
 435 refers to “not ruled out yet”.
 436

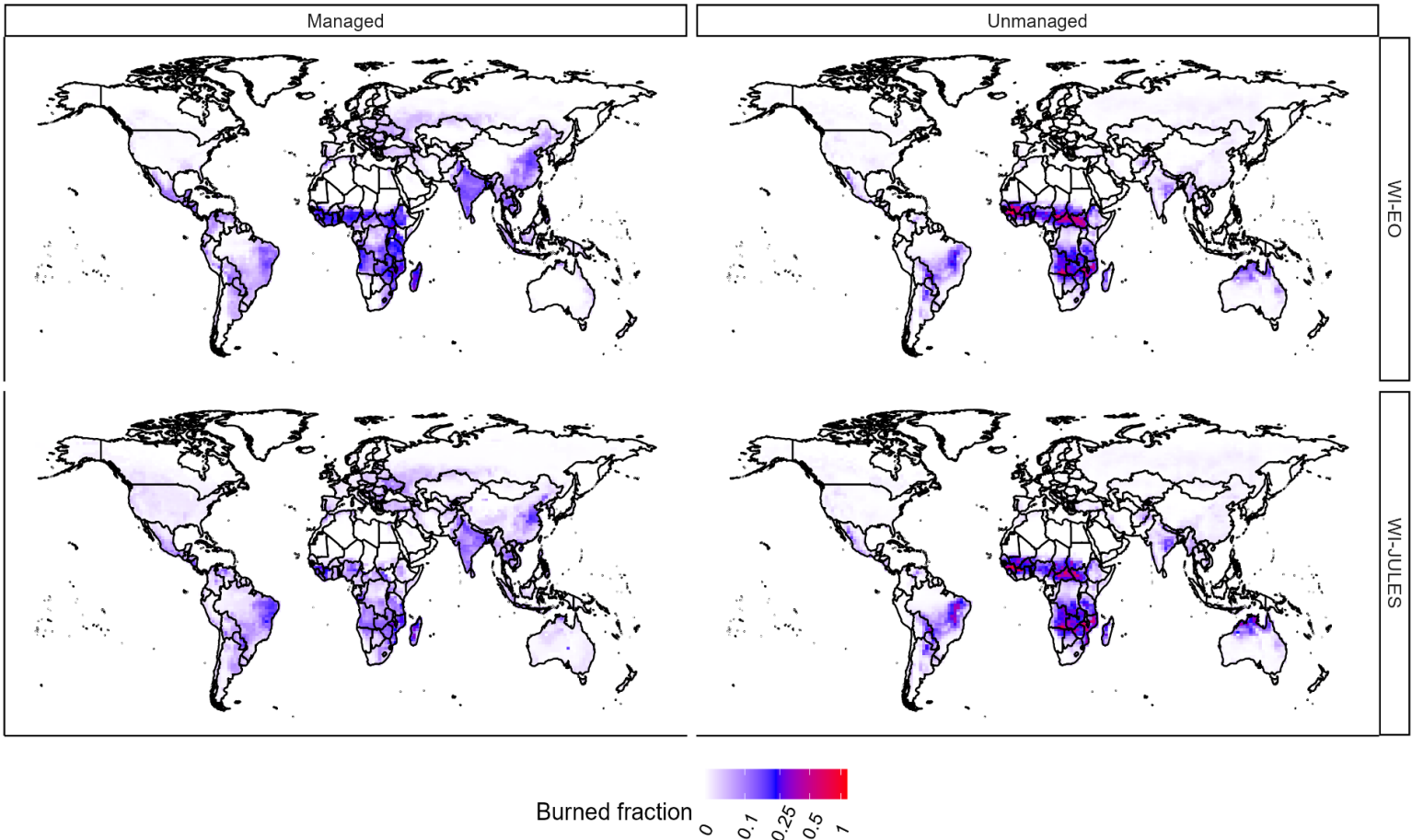
437 3.2 Analysis of WHAM-INFERNO outputs

438 3.2.1 Spatial Analysis

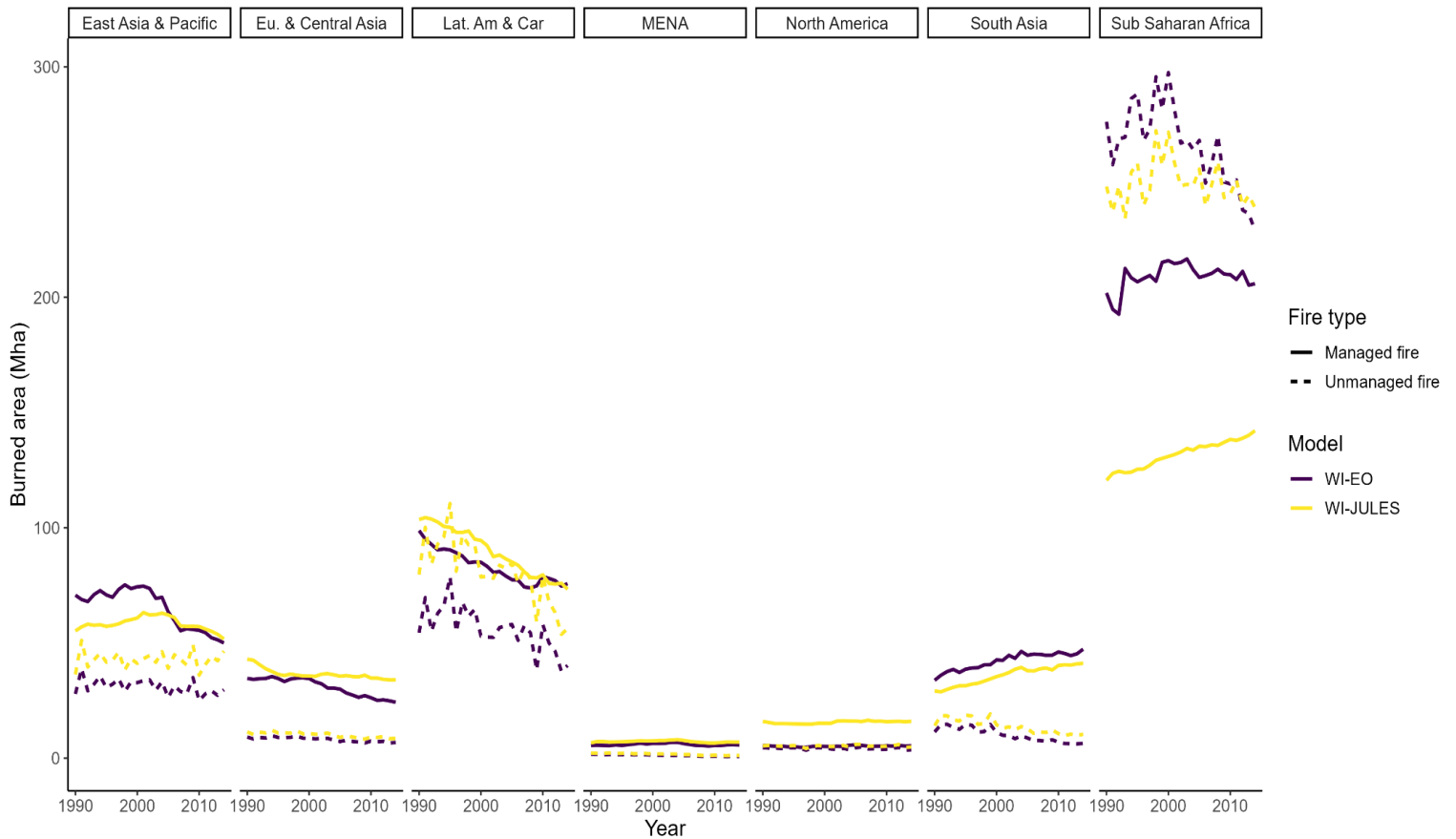
439 Across the pareto parameter runs, simulated burned area in both coupled models is split
440 approximately evenly between managed and unmanaged fires. Over the historical period (1990-
441 2014) in WI-JULES a mean of 442 Mha (54%) comes from unmanaged fires and 379 Mha
442 (46%) from managed fires. Similarly, in WI-EO, 405 Mha (47%) comes from unmanaged fires,
443 and 453 Mha (53%) comes from managed fires.

444 Furthermore, there is substantial heterogeneity in the spatial location of burned area due
445 to managed *versus* unmanaged fires (Figure 4). For example, across 1990-2014 at the level of
446 World Bank regions, in sub-Saharan Africa WI-JULES suggests 65% of mean annual burned
447 area is from unmanaged fires (56% in WHAM-EO; Figure 5). Conversely, in South Asia (which
448 includes India), WI-JULES suggests just 28% of burned area is from unmanaged fires (19% in
449 WI-EO; Figure 5). The predominance of managed fire is driven by large-scale crop-residue
450 burning in the region (Hall et al., 2023; Perkins et al., 2023). Furthermore, there is also regional
451 heterogeneity in the trends in managed and unmanaged fire. For example, in both WI-JULES and
452 WI-EO, managed fire is increasing in South Asia, whilst decreasing in Latin America and the
453 Caribbean (Figure 5).

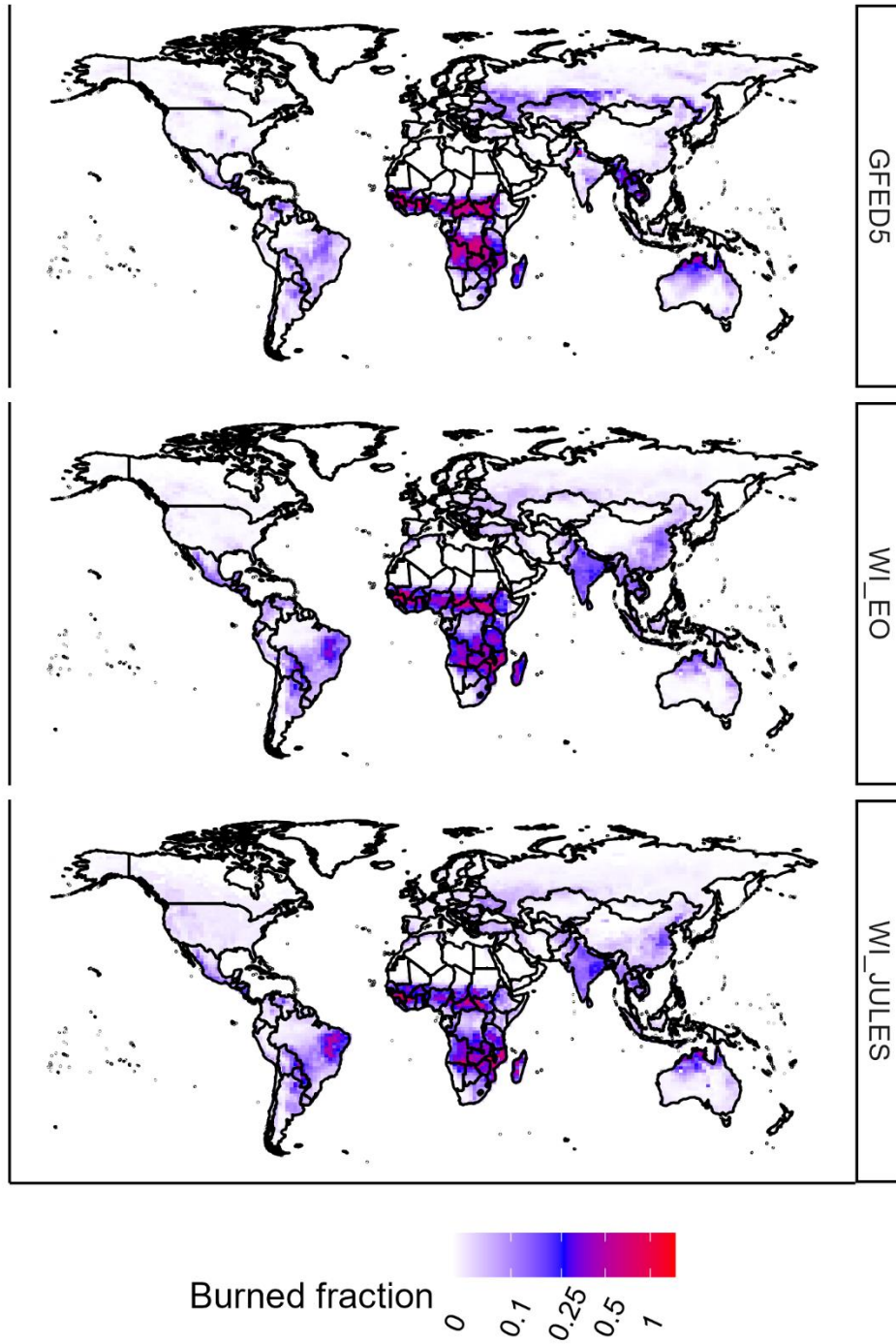
454 Perhaps the two most notable differences in sources of burned area between the two
455 models' (WI-JULES and WI-EO) simulations come in Latin America & the Caribbean and sub-
456 Saharan Africa. The difference in Latin America is that WI-JULES simulates higher unmanaged
457 burned area than WI-EO (81 Mha vs 56 Mha) particularly in the Caatinga region of Brazil
458 (Figure 6), which is due to a known anomaly in JULES' hydrological cycle in the region
459 (Perkins et al., 2023). By contrast, in sub-Saharan Africa WI-EO simulates higher unmanaged
460 burned area than WI-JULES (209 Mha vs 132 Mha), attributable to the more homogeneous
461 spatial distribution in WI-EO outputs – particularly in the Guinean Savanna – compared to the
462 comparatively heterogeneous WI-JULES outputs (Figures 4 & 6).
463



464 **Figure 4:** Distribution of managed and unmanaged fire in WHAM-INFERNO-Earth Observation
 465 (WI-EO) and WHAM-INFERNO-JULES (WI-JULES) shown as the burned fraction of each
 466 pixel. The arithmetic mean of model outputs was taken across the historical model run period
 467 (1990-2014). Principle differences between the two versions of WHAM-INFERNO are seen in
 468 the managed fire outputs of WI-EO in sub-Saharan Africa, which have a more homogeneous
 469 distribution than WI-JULES's more sporadic spatial pattern. Other anomalies between models
 470 are seen in the Caatinga region of Brazil and in the Northern Territories of Australia.
 471



472 **Figure 5:** Trends in managed and unmanaged fire across the World Bank global regions. The
 473 largest gap between managed and unmanaged fire is seen in sub-Saharan Africa, where
 474 unmanaged fire dominates. Conversely, South Asia (including India) is dominated by managed
 475 fires, particularly crop residue fires (as shown in Perkins et al., 2023). Key: Eu. & Central Asia =
 476 Europe & Central Asia; Lat. Am & Car = Latin America & Caribbean; MENA = Middle East
 477 and North Africa.
 478



479 **Figure 6:** Burned area in GFED5, WI-EO and WI-JULES as a fraction of each pixel. Values
 480 shown are the mean of the period (2001-2014). Three clear anomalies between models and
 481 GFED5 are present: firstly in the Caatinga region of Brazil, secondly in southern Russia, and
 482 thirdly in India. This latter discrepancy is due to differences in burned area from crop residue
 483 burning between WHAM! and GFED5 (Perkins et al., 2023).
 484

485 3.2.2 Temporal analysis

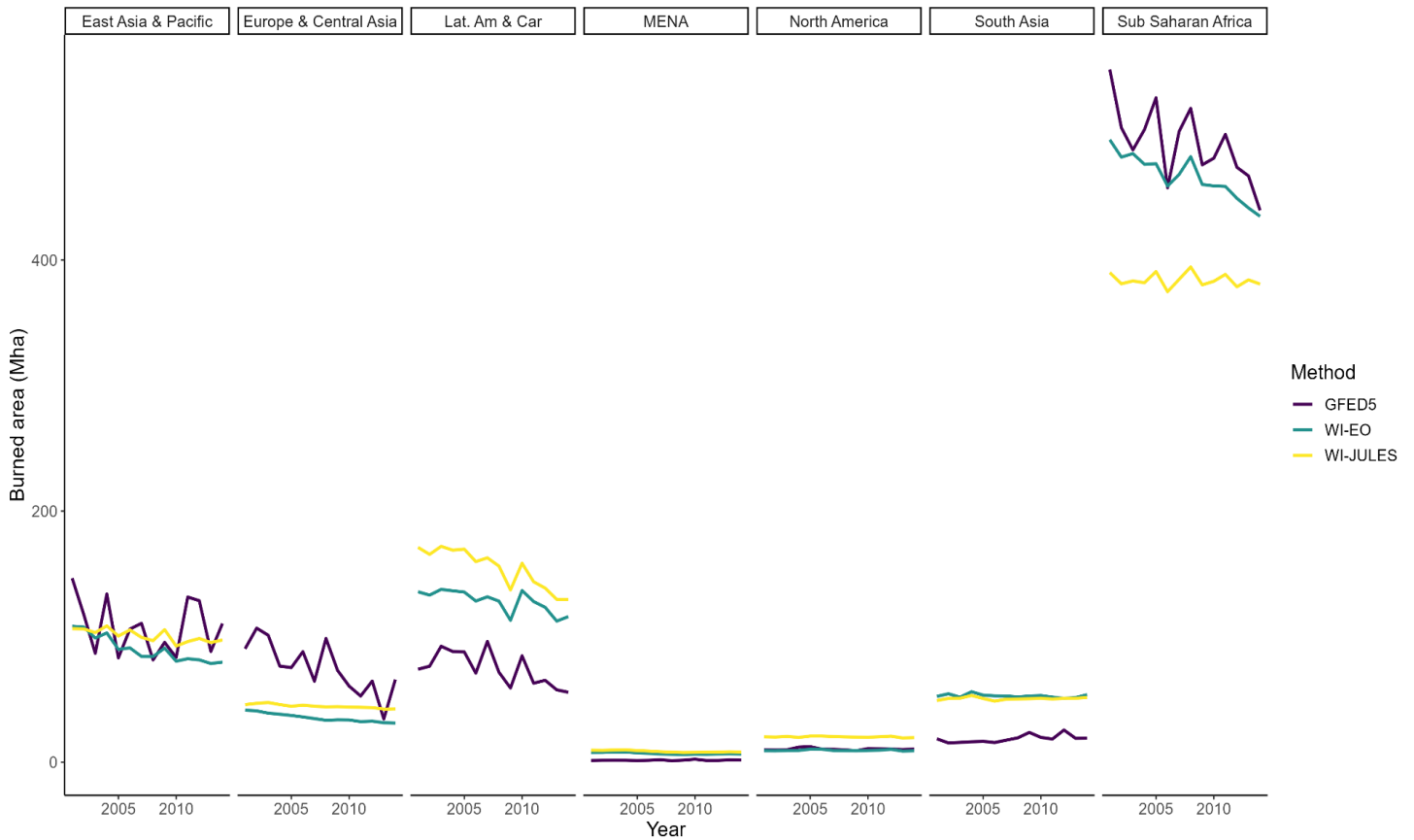
486 Across the overlapping period with GFED5 (2001-2014), WI-EO global burned area
487 declines by 137 Mha, WI-JULES burned area declines by 52 Mha, and the baseline model
488 declines by 30Mha. This compares with a decline of 193 Mha in GFED5. In WI-EO, this global
489 decline is primarily attributable to the trend in sub-Saharan Africa (Figure 7), where burned area
490 declines by 61 Mha (compared to 112 Mha in GFED5). By contrast, in WI-JULES burned area
491 in sub-Saharan Africa declines by just 9 Mha (Figure 7). This lack of decline in sub-Saharan
492 Africa is in part due to managed fires, which increase by 10 Mha as crop residue burning
493 increases in the region in this model. A similar trend is seen in sub-Saharan African crop-residue
494 burning in WI-EO, but this is offset by a steeper decline in pasture fires (Perkins et al., 2023).
495 Further, WI-JULES seemingly overestimates the rate of declining burned area in Latin America
496 & Caribbean (-42 Mha; GFED5 -18 Mha), whilst WI-EO captures a similar rate of decline to
497 GFED5 (-20 Mha). As such, WI-EO is best able to reproduce the observed decline in burned
498 area, followed by WI-JULES, and then the baseline model. The drivers of this modelled decline
499 are explored in detail below.

500 Globally, both WI-JULES and WI-EO underestimate the magnitude of interannual
501 variability (IAV) in burned area. The standard deviation of detrended model outputs (i.e. with
502 mean = 0) was 9.5Mha in WI-EO and 9.7Mha in WI-JULES. However, the correlation of the
503 detrended outputs with GFED5 was 0.81 in WI-EO and 0.41 in WI-JULES: indicating that
504 although the magnitude of IAV is underestimated in both models, WI-EO is substantially better
505 at capturing the direction of fluctuations in burned area. IAV in both model is driven by
506 unmanaged fire. Detrended global outputs for unmanaged fire correlate with detrended global
507 burned area in GFED5 (WI-EO: $r = 0.74$, WI-JULES: $r = 0.53$); however there is no meaningful
508 relationship for IAV in GFED5 and detrended outputs for managed fire ($r \leq 0.11$).

509 Based on the variable with the strongest Kendall's Tau correlation in each pixel, inter-
510 annual change in burned area due to unmanaged fire is most strongly associated with
511 flammability (Figure 8). In WI-JULES, flammability has the highest Tau value across 9,644 Mha
512 (~70% of global land area; Table 2), whilst cropland conversion, which has the strongest
513 relationship over the second largest area, has the highest Tau value across 1,037 Mha (~8% of
514 global land area). A similar trend is seen in WI-EO, where flammability has the highest Tau
515 value across 9,414 Mha and cropland conversion has the highest Tau value across 1,052 Mha.

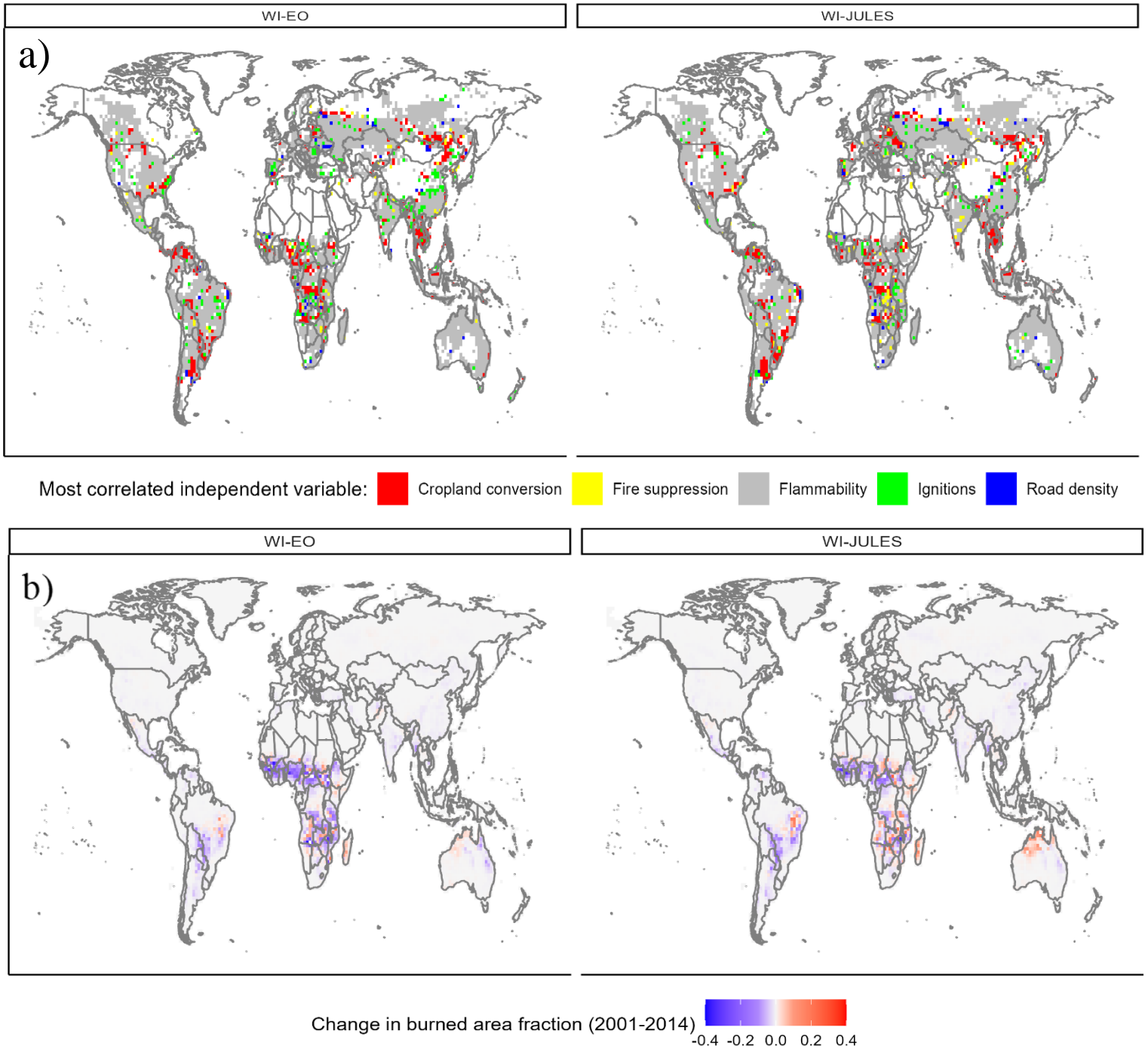
516 However, whilst change in burned area is most closely correlated with flammability over
517 the largest area, these areas are seemingly weighted towards model pixels with less overall
518 change in burned area. For both WI-EO and WI-JULES, in linear regression models of
519 interannual variability absolute t-values for flammability are more than twice as large as any
520 other variable (Table 2). By contrast, for the overall change over 2001-2014, t-values are closer
521 between variables, with ignitions having the largest absolute t-values for both models. Similarly,
522 variables with a negative impact on burned area have a larger impact on the overall 2001-2014
523 change than interannual variation (Table 2). Road density seemingly has the largest impact on
524 declining burned area (t-values: -21.7 & -19.3), followed by cropland conversion (t-values: -16.1
525 & -19.1) respectively. Fire suppression has only a marginal influence and indeed shows little
526 relationship with the long-term trend in WI-JULES ($t = 0.433$).

527



528

529 **Figure 7:** Burned area by World Bank region in GFED5 and the two versions of the WHAM-
 530 INFERNO model ensemble (WHAM-EO, WI-JULES). WI-EO is best able to reproduce the
 531 observed decline in burned area in sub-Saharan Africa, with WI-JULES showing an essentially
 532 static burned area. Conversely, both WI-EO and WI-JULES overestimate burned area in Latin
 533 America, though the trend of declining burned area is captured strongly. Both models show
 534 generally poor performance in Europe & Central Asia, showing limited discernible trend. Model
 535 outputs for WI-EO and WI-JULES are the sum of the managed and unmanaged burned area
 536 presented in Figure 5. Key: Lat. Am & Car = Latin America & Caribbean; MENA = Middle East
 537 and North Africa.



538 **Figure 8:** Relationship of changes in unmanaged burned area to independent variables. a)
 539 Variable with highest absolute correlation (τ) with change in burned area from unmanaged fire;
 540 values were filtered for pixels with at least 0.1% of the land area burned. b) Change in burned
 541 area between 2001-2014. Although flammability is most closely correlated with changes in
 542 burned area across the largest geographic space, the influence of other factors – particularly
 543 cropland conversion – is clustered towards pixels with the largest changes in burned area. A non-
 544 linear stretch was applied to the colour scale in b) to show differences between smaller absolute
 545 values.

546 **Table 2:** Relationship of changes in burned area from unmanaged fires to explanatory variables.
 547 Area gives the total land surface over which each variable was most strongly correlated with
 548 changing burned area. T-values are from linear models of change in burned area to change in the
 549 independent variable; IAV (interannual variation) is for linear models of year-on-year change
 550 between 2001-2014, whilst trend denotes overall change during the same period.

551

	WI-EO (area; Mha)	WI-EO (t-value; IAV)	WI-EO (t-value; trend)	WI-JULES (area; Mha)	WI-JULES (t-value; IAV)	WI-JULES (t-value; trend)
Cropland conversion	1052	-10.4	-16.1	1037	-13.8	-19.1
Fire suppression	244	-2.78	3.26	377	-1.9	0.43
Flammability	9414	162.3	24.4	9644	267.2	46.0
Ignitions	736	70.61	25.7	522	87.5	46.6
Road density	206	-5.1	-21.7	209	-8.0	-19.3

552

553 **4 Discussion**

554 This paper has presented the first integration of a global-scale behavioural model of
 555 human fire use and management coupled with a dynamic global vegetation model. Discussion
 556 focuses on advances made for global understanding of human drivers of vegetation fire regimes
 557 through this technical advance, before addressing its limitations and possible future directions for
 558 development of WHAM-INFERNO.

559 **4.1 WHAM-INFERNO: Insights for global-human fire interactions**

560 The WHAM-INFERNO model integration reveals both the extent and the diversity of the
 561 socio-ecological dynamics of global fire regimes. In pareto model runs of WHAM-INFERNO,
 562 managed and unmanaged fire contribute approximately equal amounts of global burned area.
 563 Furthermore, the spatiotemporal distribution of anthropogenic managed fire, and its relationship
 564 with unmanaged ('wild') fires differs substantially across space. Whilst anthropogenic fire use,
 565 primarily for crop residue burning, dominates the South Asian World Bank Region, in sub-
 566 Saharan Africa more than half of burned area is from unmanaged fires (Figure 5). Such
 567 differences have profound implications for understanding of global fire regimes and illustrates
 568 that effective fire management policies and climate adaptation strategies must be based on
 569 detailed understanding of how human livelihoods and associated fire use systems contribute to
 570 existing fire regimes. At the very least, the large extent of managed anthropogenic fire around
 571 the world implied by these results is demonstration of the inadequacy of model approaches
 572 seeking to represent direct anthropogenic influence on fire regimes as simple functions of
 573 population density (Rabin et al., 2017).

574

575 Furthermore, combined global-scale simulations of both managed and unmanaged fire
576 presented here add weight to the finding from Earth observation that small fires have declined
577 less than larger ones (Chen et al., 2023). Managed fire declines by just 35% and 52% of the rate
578 of unmanaged fire in WI-JULES and WI-EO respectively. Data from empirical studies indicates
579 that the two largest sources of burned area from managed human fires – crop residue burning and
580 pasture management – have mean sizes of 5 ha and 34 ha respectively (Millington et al., 2022),
581 whilst in JULES-INFERNO mean burned area per fire for unmanaged fires varies from 170 ha to
582 320 ha. This result seems to give weight to findings of Smith et al., (2022) and Perkins et al.,
583 (2023), that managed fire is changing in line with socio-ecological forces that are distinct from
584 those driving change in unmanaged fire.

585 In addition, the finding that unmanaged fire is primarily responsible for interannual
586 variability in burned area (Section 3.2.2) is consistent with the findings of Randerson et al.,
587 (2012), who find less fluctuation in small fires than those detectable by MODIS (i.e. <21 ha).
588 This is intuitive, as crop residue fires, for example, occur annually according to the logic of
589 cropping systems rather than fluctuations in climate (Millington et al., 2022). However, this
590 opens an intriguing possibility for fire-enabled DGVMs, which have typically struggled with
591 interannual variability whilst also not including representation of managed human fires – the
592 more static part of the regime (Li et al., 2019). In effect, DGVMs may have been *doubly*
593 underestimating the sensitivity of burned area from unmanaged fires to interannual climate
594 variability. This underrepresentation of the sensitivity of unmanaged fires to climate volatility
595 may contribute to the difficulty of attributing changes in global fire regimes to global warming
596 (Jones et al., 2022), although a lack of representation of peat fires may also be a partial
597 explanation (Blackford et al., 2023; Li et al., 2019).

598 By accounting for the less temporally variable and more spatially homogeneous signal of
599 burned area due to managed fires (Figures 4 & 5), the WHAM-INFERNO integration advances
600 understanding of the drivers of declining global burned area. Whilst interannual variability is
601 primarily driven by changes in vegetation flammability, longer-term change in burned area
602 highlights the important role played by the fragmentation of natural and semi-natural vegetation
603 through road building and cropland conversion (Figure 8). This result coheres strongly with that
604 of Andela et al., (2017) who find that interannual variability is closely linked to precipitation,
605 whilst cropland fraction is strongly associated with declining burned area. Furthermore, WHAM-
606 INFERNO can identify the processes underlying the finding of Andela that cropland has a
607 spatially heterogeneous impact on burned area. For example, increased burned area in croplands
608 in South Asia and Northeastern China is due to large-scale agricultural residue burning, whilst
609 decreased fire in savanna grasslands is due to landscape fragmentation and the subsequent
610 reduced capacity of savanna grasslands to sustain unmanaged fires.
611

612 4.2 Model performance and limitations

613 Both versions of the WHAM-INFERNO ensemble represent a significant improvement in
614 the capacity of INFERNO to reproduce historical global annual burned area over the baseline
615 model (Figure 3), and indeed over the performance of INFERNO against GFED4 presented in
616 FIREMIP ($r=0.70$; Mangeon et al., 2016; Teckentrup et al., 2019). This demonstrates the
617 fundamental importance of a process-based approach to understanding and representing human-
618 fire interactions in global modelling. Furthermore, the improvements made in WHAM-
619 INFERNO over the baseline version allow the impact of landscape fragmentation in global
620 burned area to be incorporated and understood (Figures 2 & 8). Indeed, the WHAM-INFERNO
621 integration, and particular WI-EO seems to advance capacity for DGVMs to reproduce the
622 observed decline in global burned area (Hantson et al., 2020).

623 However, representation of landscape fragmentation, its interaction with different
624 ecosystem types, and other anthropogenic pressures remains incomplete. One way that WHAM-
625 INFERNO represents fragmentation is through the role of roads in reducing fire size (Haas et al.,
626 2022), by applying a road density correction to fire sizes per PFT. Although useful in
627 constraining the model pareto parameter space through restricting burned area in more densely
628 populated areas (Supplementary Information; Figure S1) this single global function is a
629 somewhat simplistic way of capturing such effects, resulting in a substantially larger impact on
630 WHAM-INFERNO burned area outputs than on correlation with GFED5 (Supplementary
631 Information; Figure S2). Hence, the road density parameterisation in WHAM-INFERNO
632 employed to capture fragmentation effects is analogous to representations of anthropogenic
633 'ignitions' as a global function of population density in previous fire-enabled DGVMs: they are
634 both a first step with outstanding issues to be addressed. By contrast, the representation of
635 selective logging on the flammability of fire-prone tropical forests in WHAM-INFERNO has
636 been more successful. Although having a small impact on global burned area, including this
637 process leads to an improved global correlation between WHAM-INFERNO outputs and GFED5
638 (Supplementary Information; Figure S2). Representation of logging was derived from WHAM!
639 outputs, hence illustrating the value of process-based representation of anthropogenic impacts on
640 fire regimes, as opposed to the top-down road density parameterisation.

641 Finally, it is notable that WI-EO performs more strongly than WI-JULES at reproducing
642 the magnitude, spatial distribution and temporal dynamics of burned area found in GFED5. On
643 one hand, this illustrates the benefits of a well-specified parameterisation of managed human
644 fire: by better accounting for this aspect of the observed burned area signal, WI-EO is better able
645 to reproduce the inter-annual variability of unmanaged fire, and its pronounced global decline.
646 Yet the weaker performance of WI-JULES perhaps also illustrates the potential for underlying
647 error in the representation of ecosystems within DGVMs to lead to misleading conclusions being
648 drawn from their fire modules (Hantson et al., 2020). Continued model intercomparison projects
649 and use of model ensembles are likely to remain the most effective means to apply the fire
650 outputs of DGVMs (e.g. Burton et al., 2023). Overall, the large scale of anthropogenic managed
651 fire entails that careful consideration should be given to how future socioeconomic scenarios,
652 and their limitations, inform our projections of how global fire regimes may evolve under a
653 warming climate (Keys et al., 2024).

654

655 **5 Conclusion**

656 This paper has presented the first integration of a global behavioural model of human fire
657 use and management with a dynamic global vegetation model. Overall, model evaluation
658 highlights the strong benefits of coupled socio-ecological modelling approaches for reproducing
659 the observed spatial and temporal patterns of burned area globally. Furthermore, findings
660 demonstrate the extent and complexity of human-fire interactions. Results imply that managed
661 anthropogenic fire accounts for as much as half of all global burned area, whilst the trends and
662 distribution of, and relationship between, managed and unmanaged fires is highly spatially
663 heterogeneous. Such complexities demonstrate that socio-ecological modelling is vital to
664 advance understanding of present-day and future fire regimes. A key area for future work
665 identified here is in developing more nuanced representation of landscape fragmentation,
666 particularly in grazing lands in sub-Saharan Africa, which remain a central contributor to global
667 burned area.

668 **Acknowledgments**

669 This work was funded by the Leverhulme Centre for Wildfires, Environment and Society
670 through the Leverhulme Trust, grant number RC-2018-023. AV has also been supported by the
671 AXA Research Fund (project 'AXA Chair in Wildfires and Climate') and by the Hellenic
672 Foundation for Research and Innovation (Grant ID 3453). The authors declare no conflicts of
673 interest.

674 **Open Research**

675 Data and code necessary to reproduce the results in this paper, as well as analysis and
676 figures presented are made available on zenodo: <https://zenodo.org/doi/10.5281/zenodo.8319445>
677 (Perkins et al., 2023b). Code to run the WHAM-INFERNO ensemble are also made available on
678 GitHub: https://github.com/OliPerkins1987/WHAM_INFERNO. All data and code are made
679 available under a Creative Commons License.

680 **References**

- 682 Andela, N., Morton, D. C., Giglio, L., Chen, Y., van der Werf, G. R., Kasibhatla, P. S., et al.
683 (2017). A human-driven decline in global burned area. *Science*, 356(6345), 1356–1362.
684 <https://doi.org/10.1126/science.aal4108>
- 685 Archibald, S. (2016). Managing the human component of fire regimes: Lessons from Africa.
686 *Philosophical Transactions of the Royal Society B: Biological Sciences*, 371(1696),
687 20150346. <https://doi.org/10.1098/rstb.2015.0346>
- 688 Archibald, S., & Hempson, G. P. (2016). Competing consumers: Contrasting the patterns and
689 impacts of fire and mammalian herbivory in Africa. *Philosophical Transactions of the*
690 *Royal Society B: Biological Sciences*, 371(1703), 20150309.
691 <https://doi.org/10.1098/rstb.2015.0309>
- 692 Archibald, S., Staver, A. C., & Levin, S. A. (2012). Evolution of human-driven fire regimes in
693 Africa. *Proceedings of the National Academy of Sciences*, 109(3), 847–852.
694 <https://doi.org/10.1073/pnas.1118648109>

- 695 Arneth, A., Brown, C., & Rounsevell, M. D. A. (2014). Global models of human decision-
696 making for land-based mitigation and adaptation assessment. *Nature Climate Change*,
697 4(7), Article 7. <https://doi.org/10.1038/nclimate2250>
- 698 Blackford, K. R., Kasoar, M., Burton, C., Burke, E., Prentice, I. C., & Voulgarakis, A. (2023).
699 INFERNO-peat v1.0.0: A representation of northern high latitude peat fires in the
700 JULES-INFERNO global fire model. *EGUsphere*, 1–31.
701 <https://doi.org/10.5194/egusphere-2023-2399>
- 702 Burton, C., Betts, R., Cardoso, M., Feldpausch, T. R., Harper, A., Jones, C. D., et al. (2019).
703 Representation of fire, land-use change and vegetation dynamics in the Joint UK Land
704 Environment Simulator vn4.9 (JULES). *Geoscientific Model Development*, 12(1), 179–
705 193. <https://doi.org/10.5194/gmd-12-179-2019>
- 706 Burton, C., Lampe, S., Kelley, D., Thiery, W., Hantson, S., Christidis, N., et al. (2023). Global
707 burned area increasingly explained by climate change, PREPRINT (Version 1) available
708 at Research Square. <https://doi.org/10.21203/rs.3.rs-3168150/v1>
- 709 Carnell, R. (2022). *lhs: Latin Hypercube Samples*. R package version 1.1.6, [https://CRAN.R-](https://CRAN.R-project.org/package=lhs)
710 [project.org/package=lhs](https://CRAN.R-project.org/package=lhs).
- 711 Chen, Y., Hall, J., van Wees, D., Andela, N., Hantson, S., Giglio, L., et al. (2023). Multi-decadal
712 trends and variability in burned area from the 5th version of the Global Fire Emissions
713 Database (GFED5). *Earth System Science Data Discussions*, 1–52.
714 <https://doi.org/10.5194/essd-2023-182>
- 715 Christian, H. J., Blakeslee, R. J., Boccippio, D. J., Boeck, W. L., Buechler, D. E., Driscoll, K. T.,
716 et al. (2003). Global frequency and distribution of lightning as observed from space by
717 the Optical Transient Detector. *Journal of Geophysical Research: Atmospheres*, 108(D1),
718 ACL 4-1-ACL 4-15. <https://doi.org/10.1029/2002JD002347>
- 719 Clark, D. B., Mercado, L. M., Sitch, S., Jones, C. D., Gedney, N., Best, M. J., et al. (2011). The
720 Joint UK Land Environment Simulator (JULES), model description – Part 2: Carbon
721 fluxes and vegetation dynamics. *Geoscientific Model Development*, 4(3), 701–722.
722 <https://doi.org/10.5194/gmd-4-701-2011>
- 723 Cochrane, M. A., & Barber, C. P. (2009). Climate change, human land use and future fires in the
724 Amazon. *Global Change Biology*, 15(3), 601–612. [https://doi.org/10.1111/j.1365-](https://doi.org/10.1111/j.1365-2486.2008.01786.x)
725 [2486.2008.01786.x](https://doi.org/10.1111/j.1365-2486.2008.01786.x)
- 726 Driscoll, D. A., Armenteras, D., Bennett, A. F., Brotons, L., Clarke, M. F., Doherty, T. S., et al.
727 (2021). How fire interacts with habitat loss and fragmentation. *Biological Reviews*, 96(3),
728 976–998. <https://doi.org/10.1111/brv.12687>
- 729 Ford, A. E., Harrison, S. P., Kountouris, Y., Millington, J. D., Mistry, J., Perkins, O., et al.
730 (2021). Modelling human-fire interactions: Combining alternative perspectives and
731 approaches. *Frontiers in Environmental Science*, 9, 649835.
- 732 Forkel, M., Andela, N., Harrison, S. P., Lasslop, G., van Marle, M., Chuvieco, E., et al. (2019).
733 Emergent relationships with respect to burned area in global satellite observations and
734 fire-enabled vegetation models. *Biogeosciences*, 16(1), 57–76. [https://doi.org/10.5194/bg-](https://doi.org/10.5194/bg-16-57-2019)
735 [16-57-2019](https://doi.org/10.5194/bg-16-57-2019)

- 736 Giglio, L., Randerson, J. T., & van der Werf, G. R. (2013). Analysis of daily, monthly, and
737 annual burned area using the fourth-generation global fire emissions database (GFED4).
738 *Journal of Geophysical Research: Biogeosciences*, 118(1), 317–328.
739 <https://doi.org/10.1002/jgrg.20042>
- 740 Haas, O., Prentice, I. C., & Harrison, S. P. (2022). Global environmental controls on wildfire
741 burnt area, size, and intensity. *Environmental Research Letters*, 17(6), 065004.
742 <https://doi.org/10.1088/1748-9326/ac6a69>
- 743 Hall, J., Argueta, F., Zubkova, M., Chen, Y., Randerson, J. & Giglio, L. (2024). GloCAB: global
744 cropland burned area from mid-2002 to 2020. *Earth System Science Data*, 16(2), 867-
745 885. <https://doi.org/10.5194/essd-16-867-2024>
- 746 Hantson, S., Kelley, D. I., Arneth, A., Harrison, S. P., Archibald, S., Bachelet, D., et al. (2020).
747 Quantitative assessment of fire and vegetation properties in simulations with fire-enabled
748 vegetation models from the Fire Model Intercomparison Project. *Geoscientific Model
749 Development*, 13(7), 3299–3318.
- 750 Harrison, S. P., Prentice, I. C., Bloomfield, K. J., Dong, N., Forkel, M., Forrest, M., et al. (2021).
751 Understanding and modelling wildfire regimes: An ecological perspective.
752 *Environmental Research Letters*, 16(12), 125008. [https://doi.org/10.1088/1748-
753 9326/ac39be](https://doi.org/10.1088/1748-9326/ac39be)
- 754 Hijmans, R. (2023). raster: Geographic Data Analysis and Modeling. R package version 3.6-20.
755 <https://CRAN.R-project.org/package=raster>
- 756 Hurtt, G. C., Chini, L., Sahajpal, R., Frolking, S., Boudirsky, B. L., Calvin, K., et al. (2020).
757 Harmonization of global land use change and management for the period 850–2100
758 (LUH2) for CMIP6. *Geoscientific Model Development*, 13(11), 5425–5464.
759 <https://doi.org/10.5194/gmd-13-5425-2020>
- 760 Jones, M. W., Abatzoglou, J. T., Veraverbeke, S., Andela, N., Lasslop, G., Forkel, M., et al.
761 (2022). Global and Regional Trends and Drivers of Fire Under Climate Change. *Reviews
762 of Geophysics*, 60(3), e2020RG000726. <https://doi.org/10.1029/2020RG000726>
- 763 Kelley, D. I., Bistinas, I., Whitley, R., Burton, C., Marthews, T. R., & Dong, N. (2019). How
764 contemporary bioclimatic and human controls change global fire regimes. *Nature
765 Climate Change*, 9(9), 690–696. <https://doi.org/10.1038/s41558-019-0540-7>
- 766 Keys, P. W., Badia, L., & Warrier, R. (2024). The Future in Anthropocene Science. *Earth's
767 Future*, 12(1), e2023EF003820. <https://doi.org/10.1029/2023EF003820>
- 768 Kumar, N., Chaudhary, A., Ahlawat, O. P., Naorem, A., Upadhyay, G., Chhokar, R. S., et al.
769 (2023). Crop residue management challenges, opportunities and way forward for
770 sustainable food-energy security in India: A review. *Soil and Tillage Research*, 228,
771 105641. <https://doi.org/10.1016/j.still.2023.105641>
- 772 Lapola, D. M., Pinho, P., Barlow, J., Aragão, L. E. O. C., Berenguer, E., Carmenta, R., et al.
773 (2023). The drivers and impacts of Amazon forest degradation. *Science*, 379(6630),
774 eabp8622. <https://doi.org/10.1126/science.abp8622>

- 775 Laris, P. (2002). Burning the Seasonal Mosaic: Preventative Burning Strategies in the Wooded
776 Savanna of Southern Mali. *Human Ecology*, 30(2), 155–186.
777 <https://doi.org/10.1023/A:1015685529180>
- 778 Lasslop, G., Coppola, A., Voulgarakis, A., Yue, C., & Veraverbeke, S. (2019). Influence of Fire
779 on the Carbon Cycle and Climate. *Current Climate Change Reports*, 5, 112-113.
780 <https://doi.org/10.1007/s40641-019-00128-9>
- 781 Li, F., Val Martin, M., Andreae, M. O., Arneth, A., Hantson, S., Kaiser, J. W., et al. (2019).
782 Historical (1700–2012) global multi-model estimates of the fire emissions from the Fire
783 Modeling Intercomparison Project (FireMIP). *Atmospheric Chemistry and Physics*,
784 19(19), 12545–12567. <https://doi.org/10.5194/acp-19-12545-2019>
- 785 Mangeon, S., Voulgarakis, A., Gilham, R., Harper, A., Sitch, S., & Folberth, G. (2016).
786 INFERNO: A fire and emissions scheme for the UK Met Office's Unified Model.
787 *Geoscientific Model Development*, 9(8), 2685–2700. [https://doi.org/10.5194/gmd-9-2685-](https://doi.org/10.5194/gmd-9-2685-2016)
788 2016
- 789 Mathison, C., Burke, E., Hartley, A. J., Kelley, D. I., Burton, C., Robertson, E., et al. (2023).
790 Description and evaluation of the JULES-ES set-up for ISIMIP2b. *Geoscientific Model*
791 *Development*, 16(14), 4249–4264. <https://doi.org/10.5194/gmd-16-4249-2023>
- 792 Meijer, J. R., Huijbregts, M. A. J., Schotten, K. C. G. J., & Schipper, A. M. (2018). Global
793 patterns of current and future road infrastructure. *Environmental Research Letters*, 13(6),
794 064006. <https://doi.org/10.1088/1748-9326/aabd42>
- 795 Millington, J. D. A., Perkins, O., & Smith, C. (2022). Human Fire Use and Management: A
796 Global Database of Anthropogenic Fire Impacts for Modelling. *Fire*, 5(4), Article 4.
797 <https://doi.org/10.3390/fire5040087>
- 798 Perkins, O., Kasoar, M., Voulgarakis, A., Smith, C., Mistry, J., & Millington, J. (2023). A global
799 behavioural model of human fire use and management: WHAM! v1.0. *EGUsphere*
800 (accepted for publication in *Geoscientific Model Development*), 1–42.
801 <https://doi.org/10.5194/egusphere-2023-2162>.
- 802 Perkins, O., Kasoar, M., Voulgarakis, A., Edwards, T., & Millington, J. (2023b). [Software]
803 WHAM-INFERNO, code and supporting data.
804 <https://zenodo.org/doi/10.5281/zenodo.8319445>
- 805 Perkins, O., & Millington, J. D. A. (2021). DAFI: A global database of Anthropogenic Fire.
806 *Figshare* <https://doi.org/10.6084/M9.Figshare.c.5290792>.
- 807 R Core Team. (2022). R: A language and environment for statistical computing. R Foundation
808 for Statistical Computing, Vienna, Austria. <https://www.R-project.org/>.
- 809 Rabin, S. S., Melton, J. R., Lasslop, G., Bachelet, D., Forrest, M., Hantson, S., et al. (2017). The
810 Fire Modeling Intercomparison Project (FireMIP), phase 1: Experimental and analytical
811 protocols with detailed model descriptions. *Geoscientific Model Development*, 10(3),
812 1175–1197. <https://doi.org/10.5194/gmd-10-1175-2017>
- 813 Randerson, J. T., Chen, Y., van der Werf, G. R., Rogers, B. M., & Morton, D. C. (2012). Global
814 burned area and biomass burning emissions from small fires. *Journal of Geophysical*
815 *Research: Biogeosciences*, 117(G4). <https://doi.org/10.1029/2012JG002128>

- 816 Ripley, B. S., Raubenheimer, S. L., Perumal, L., Anderson, M., Mostert, E., Kgope, B. S.,
817 Midgley, G. F., & Simpson, K. J. (2022). CO₂-fertilisation enhances resilience to
818 browsing in the recruitment phase of an encroaching savanna tree. *Functional Ecology*,
819 36(12), 3223–3233. <https://doi.org/10.1111/1365-2435.14215>
- 820 Robinson, D. T., Di Vittorio, A., Alexander, P., Arneeth, A., Barton, C. M., Brown, D. G.,
821 Kettner, A., Lemmen, C., et al. (2018). Modelling feedbacks between human and natural
822 processes in the land system. *Earth System Dynamics*, 9(2), 895–914.
823 <https://doi.org/10.5194/esd-9-895-2018>
- 824 Rosan, T. M., Sitch, S., Mercado, L. M., Heinrich, V., Friedlingstein, P., & Aragão, L. E. O. C.
825 (2022). Fragmentation-Driven Divergent Trends in Burned Area in Amazonia and
826 Cerrado. *Frontiers in Forests and Global Change*, 5.
827 <https://www.frontiersin.org/articles/10.3389/ffgc.2022.801408>
- 828 Rougier, J. C., & Beven, K. J. (2013). *Model and data limitations: The sources and implications*
829 *of epistemic uncertainty* (pp. 40–63). Cambridge University Press.
830 <https://doi.org/10.1017/CBO9781139047562.004>
- 831 Shuman, J. K., Balch, J. K., Barnes, R. T., Higuera, P. E., Roos, C. I., Schwilk, D. W., et al.
832 (2022). Reimagine fire science for the anthropocene. *PNAS Nexus*, 1(3), pgac115.
833 <https://doi.org/10.1093/pnasnexus/pgac115>
- 834 Smith, C., Perkins, O., & Mistry, J. (2022). Global decline in subsistence-oriented and
835 smallholder fire use. *Nature Sustainability*, 5(6), Article 6.
836 <https://doi.org/10.1038/s41893-022-00867-y>
- 837 Stevens, N., Erasmus, B. F. N., Archibald, S., & Bond, W. J. (2016). Woody encroachment over
838 70 years in South African savannahs: Overgrazing, global change or extinction
839 aftershock? *Philosophical Transactions of the Royal Society B: Biological Sciences*,
840 371(1703), 20150437. <https://doi.org/10.1098/rstb.2015.0437>
- 841 Teckentrup, L., Harrison, S. P., Hantson, S., Heil, A., Melton, J. R., Forrest, M., et al. (2019).
842 Response of simulated burned area to historical changes in environmental and
843 anthropogenic factors: A comparison of seven fire models. *Biogeosciences*, 16(19),
844 3883–3910. <https://doi.org/10.5194/bg-16-3883-2019>
- 845 UNEP - the United Nations Environment Programme (2022). *Spreading like Wildfire: The*
846 *Rising Threat of Extraordinary Landscape Fires*.
847 [http://www.unep.org/resources/report/spreading-wildfire-rising-threat-extraordinary-](http://www.unep.org/resources/report/spreading-wildfire-rising-threat-extraordinary-landscape-fires)
848 [landscape-fires](http://www.unep.org/resources/report/spreading-wildfire-rising-threat-extraordinary-landscape-fires)
- 849 Wiltshire, A. J., Duran Rojas, M. C., Edwards, J. M., Gedney, N., Harper, A. B., Hartley, A. J.,
850 et al. (2020). JULES-GL7: The Global Land configuration of the Joint UK Land
851 Environment Simulator version 7.0 and 7.2. *Geoscientific Model Development*, 13(2),
852 483–505. <https://doi.org/10.5194/gmd-13-483-2020>
- 853 Zubkova, M., Humber, M. L., & Giglio, L. (2023). Is global burned area declining due to
854 cropland expansion? How much do we know based on remotely sensed data?
855 *International Journal of Remote Sensing*, 44(4), 1132–1150.
856 <https://doi.org/10.1080/01431161.2023.2174389>
857

858 **References from the supporting information**

- 859 Craig, P.S., Goldstein, M., Seheult, A.H., & Smith, J.A. (1997). *Pressure Matching for*
860 *Hydrocarbon Reservoirs: A Case Study in the Use of Bayes Linear Strategies for Large*
861 *Computer Experiments*, in: Gatsonis, C., Hodges, J.S., Kass, R.E., McCulloch, R., Rossi,
862 P., Singpurwalla, N.D. (Eds.), *Case Studies in Bayesian Statistics*, Lecture Notes in
863 Statistics. Springer, New York, NY, pp. 37–93. [https://doi.org/10.1007/978-1-4612-2290-](https://doi.org/10.1007/978-1-4612-2290-3_2)
864 [3_2](https://doi.org/10.1007/978-1-4612-2290-3_2)
- 865 Florian, A. (1992). An efficient sampling scheme: Updated Latin Hypercube Sampling.
866 *Probabilistic Engineering Mechanics*, 7, 123–130. [https://doi.org/10.1016/0266-](https://doi.org/10.1016/0266-8920(92)90015-A)
867 [8920\(92\)90015-A](https://doi.org/10.1016/0266-8920(92)90015-A)
- 868 Gupta, H.V., Sorooshian, S., & Yapo, P.O., 1998. Toward improved calibration of hydrologic
869 models: Multiple and noncommensurable measures of information. *Water Resources*
870 *Research*, 34, 751–763. <https://doi.org/10.1029/97WR03495>
- 871 Kennedy, M., & O'Hagan, A. (2001). Bayesian calibration of computer models, *Journal of the*
872 *Royal Statistical Society B*, 63:3, 425-464.
- 873 Lin, Y., Xu, D., Wang, N., Shi, Z., & Chen, Q. (2020). Road Extraction from Very-High-
874 Resolution Remote Sensing Images via a Nested SE-Deeplab Model. *Remote Sensing*, 12,
875 2985. <https://doi.org/10.3390/rs12182985>
- 876 Lu, L., Anderson-Cook, C.M., & Robinson, T.J. (2011). Optimization of Designed Experiments
877 Based on Multiple Criteria Utilizing a Pareto Frontier. *Technometrics*, 53, 353–365.
- 878 McNeill, D., Williams, J., Booth, B., Betts, R., Challenor, P., Wiltshire, A., & Sexton, D. (2016).
879 The impact of structural error on parameter constraint in a climate model. *Earth System*
880 *Dynamics*, 7, 917–935. <https://doi.org/10.5194/esd-7-917-2016>
- 881 Pukelsheim, F. (1994). The Three Sigma Rule. *The American Statistician*, 48, 88–91.
882 <https://doi.org/10.2307/2684253>
- 883 Roteta, E., Bastarrika, A., Padilla, M., Storm, T., & Chuvieco, E. (2019). Development of a
884 Sentinel-2 burned area algorithm: Generation of a small fire database for sub-Saharan
885 Africa. *Remote Sensing of Environment*, 222, 1–17.
886 <https://doi.org/10.1016/j.rse.2018.12.011>
- 887 Williamson, D., Goldstein, M., Allison, L., Blaker, A., Challenor, P., Jackson, L., & Yamazaki,
888 K. (2013). History matching for exploring and reducing climate model parameter space
889 using observations and a large perturbed physics ensemble. *Climate Dynamics*, 41, 1703–
890 1729. <https://doi.org/10.1007/s00382-013-1896-4>

891

892